Report

Current Biology

S-acylation stabilizes ligand-induced receptor kinase complex formation during plant pattern-triggered immune signaling

Graphical abstract

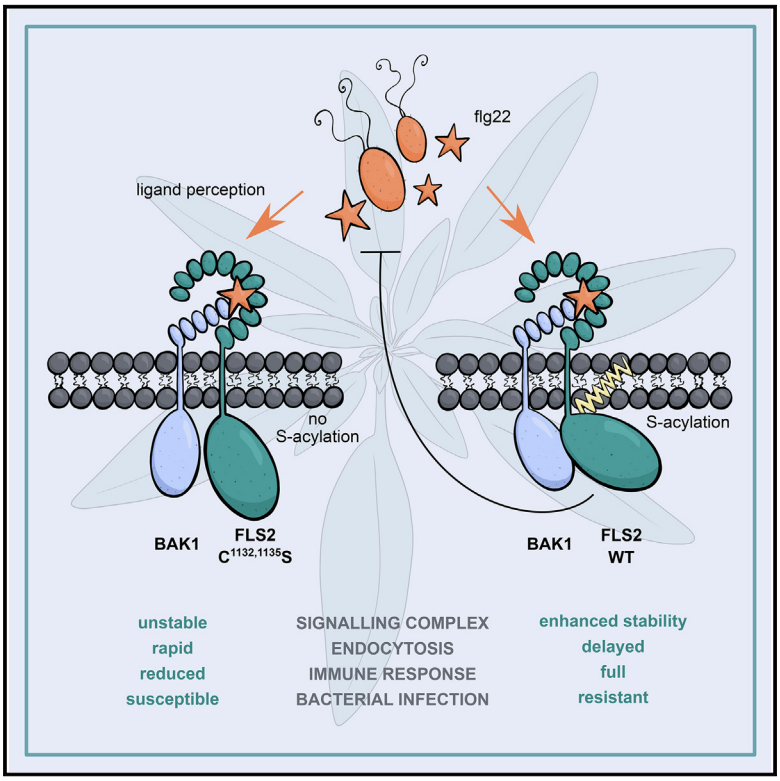

Highlights

- FLS2 and EFR are S-acylated in response to ligand binding
- FLS2 S-acylation stabilizes FLS2-BAK1 interactions at the plasma membrane
- FLS2 S-acylation delays endocytosis of activated FLS2 complexes
- FLS2 S-acylation is essential for immunity against bacterial pathogens

Authors

Charlotte H. Hurst, Dionne Turnbull, Kaltra Xhelilaj, ..., Cyril Zipfel, Julien Gronnier, Piers A. Hemsley

Correspondence

p.a.hemsley@dundee.ac.uk

In brief

Hurst et al. show that the plant pathogen-perceiving receptors, FLS2 and EFR, undergo ligand-responsive modification by fatty acids (S-acylation) at a kinase domain cysteine residue conserved in all plant receptor kinases. S-acylation acts to stabilize active receptor complexes and prolong signaling from the plasma membrane to promote immunity.

Hurst et al., 2023, Current Biology *33*, 1–9
April 24, 2023
https://doi.org/10.1016/j.cub.2023.02.065

CellPress

Please cite this article in press as: Hurst et al., S-acylation stabilizes ligand-induced receptor kinase complex formation during plant pattern-triggered immune signaling, Current Biology (2023), https://doi.org/10.1016/j.cub.2023.02.065

Current Biology

CellPress

Report

S-acylation stabilizes ligand-induced receptor kinase complex formation during plant pattern-triggered immune signaling

Charlotte H. Hurst,[1,2] Dionne Turnbull,[1] Kaltra Xhelilaj,[3] Sally Myles,[1] Robin L. Pflughaupt,[4] Michaela Kopischke,[5] Paul Davies,[4] Susan Jones,[6] Silke Robatzek,[5,8] Cyril Zipfel,[5,7] Julien Gronnier,[3,7] and Piers A. Hemsley[1,2,9,10,*]

[1]Division of Plant Sciences, School of Life Sciences, University of Dundee, Dow Street, Dundee DD1 5EH, UK
[2]Cell and Molecular Sciences, The James Hutton Institute, Invergowrie, Dundee DD2 5DA, UK
[3]ZMBP Universität Tübingen, Auf der Morgenstelle 32, 72076 Tübingen, Germany
[4]Medical Research Council Protein Phosphorylation and Ubiquitylation Unit, School of Life Sciences, University of Dundee, Dow Street, Dundee DD1 5EH, UK
[5]The Sainsbury Laboratory, University of East Anglia, Norwich Research Park, Norwich NR4 7UH, UK
[6]Information and Computational Sciences, The James Hutton Institute, Invergowrie, Dundee DD2 5DA, UK
[7]Institute of Plant and Microbial Biology, Zurich-Basel Plant Science Center, University of Zurich, 8008 Zurich, Switzerland
[8]Present address: LMU Munich Biocenter, Großhadener Strasse 4, 82152 Planegg, Germany
[9]Twitter: @Hemsley_Lab
[10]Lead contact
*Correspondence: p.a.hemsley@dundee.ac.uk
https://doi.org/10.1016/j.cub.2023.02.065

SUMMARY

Plant receptor kinases are key transducers of extracellular stimuli, such as the presence of beneficial or pathogenic microbes or secreted signaling molecules. Receptor kinases are regulated by numerous post-translational modifications.[1–3] Here, using the immune receptor kinases FLS2[4] and EFR,[5] we show that S-acylation at a cysteine conserved in all plant receptor kinases is crucial for function. S-acylation involves the addition of long-chain fatty acids to cysteine residues within proteins, altering their biochemical properties and behavior within the membrane environment.[6] We observe S-acylation of FLS2 at C-terminal kinase domain cysteine residues within minutes following the perception of its ligand, flg22, in a BAK1 co-receptor and PUB12/13 ubiquitin ligase-dependent manner. We demonstrate that S-acylation is essential for FLS2-mediated immune signaling and resistance to bacterial infection. Similarly, mutating the corresponding conserved cysteine residue in EFR suppressed elf18-triggered signaling. Analysis of unstimulated and activated FLS2-containing complexes using microscopy, detergents, and native membrane DIBMA nanodiscs indicates that S-acylation stabilizes, and promotes retention of, activated receptor kinase complexes at the plasma membrane to increase signaling efficiency.

RESULTS

Receptor kinases (RKs) found in the plant plasma membrane act as the principle means of perception for most extracellular physical stimuli, such as hormones, signaling peptides, and microbe-associated molecular patterns (MAMPs). RKs comprise the largest single gene family in plants[7,8] and are central to current efforts to breed or engineer crops able to withstand emerging pathogen threats, interact with beneficial microbes, or better tolerate abiotic stress.[9–12] Understanding mechanisms and principles underpinning the behavior of RKs is therefore critical to informing these approaches.

The RK FLAGELLIN SENSING 2 (FLS2) is the receptor for bacterial flagellin[13] and is an archetype for RK research, particularly for host-microbe interactions. Flagellin binding to the extracellular leucine-rich repeats of FLS2 induces interaction with the co-receptor BRI1-ASSOCIATED RECEPTOR KINASE 1/SOMATIC EMBRYOGENESIS RECEPTOR-LIKE KINASE 3 (BAK1/SERK3). Subsequent transphosphorylation of FLS2 by BAK1 initiates a cascade of immune signaling to activate anti-bacterial defense responses. As part of this overall process, changes in FLS2 phosphorylation,[3] SUMOylation,[1] and ubiquitination[2] state occur, indicating a high degree of post-translational regulation. FLS2 activation also alters the overall complex composition[1,2,13–21] and physical properties.[22] However, the mechanisms and relevance of these changes remain largely unknown.

S-acylation is a reversible post-translational modification, whereby long-chain fatty acids are added to cysteine residues by protein S-acyl transferases[23] and removed by acyl-protein thioesterases.[24] This modification can lead to changes in protein trafficking, stability, and turnover, and S-acylation has been proposed to drive membrane phase partitioning.[25,26] While changes in protein S-acylation state are hypothesized to modulate protein-protein and protein-membrane interactions, or alter protein activation states,[6] direct experimental evidence is lacking.

Please cite this article in press as: Hurst et al., S-acylation stabilizes ligand-induced receptor kinase complex formation during plant pattern-triggered immune signaling, Current Biology (2023), https://doi.org/10.1016/j.cub.2023.02.065

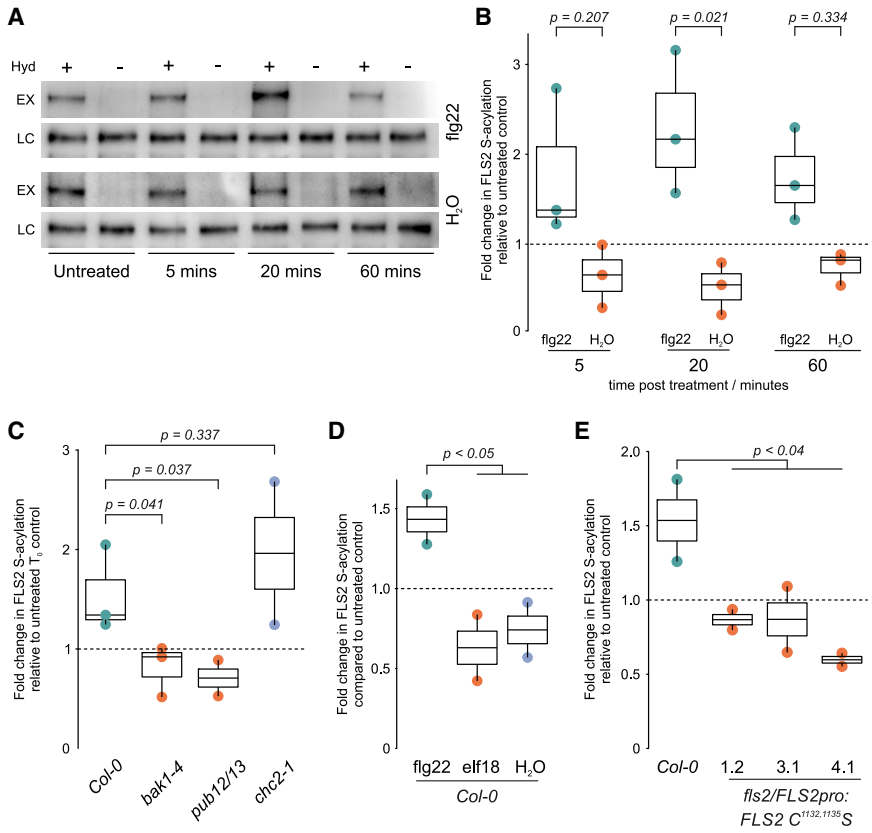

Figure 1. FLS2 S-acylation increases upon flg22 perception

(A) Representative western blot of FLS2 S-acylation state in *Arabidopsis* Col-0 plants treated with 1 μM flg22 peptide or water, as determined by acyl-biotin exchange assay. EX, S-acylation state; LC, loading control; Hyd, presence (+) or absence (–) of hydroxylamine.

(B) Quantification of western blot data in (A) showing change in S-acylation state in *Arabidopsis* Col-0 plants treated with 1 μM flg22 (green) or water (orange). S-acylation state is shown relative to untreated plants (black dashed line). n = 3 biological repeats. Box plot shows median and IQR; whiskers indicate data points within 1.5 × IQR. Significance of difference between flg22 and water treatments at each time point was determined by ANOVA and Tukey's HSD test.

(C) S-acylation of FLS2 in response to flg22 requires BAK1 and PUB12/13 but not CHC2. S-acylation state was determined by acyl-biotin exchange after 20 min exposure to 1 μM flg22 and is shown relative to untreated *Arabidopsis* plants of the same genotype (dashed line). Box plot shows median and IQR, whiskers indicate data points within 1.5 × IQR. Significant differences of each genotype to flg22-treated *Arabidopsis* Col-0, as determined by Student's t test, are shown.

(D) FLS2 undergoes S-acylation in response to flg22 treatment but not elf18. S-acylation state as determined by acyl-biotin exchange after 20 min of treatment using 1 μM peptide or water is shown relative to untreated *Arabidopsis* plants (black, dashed line). Box plot shows median and IQR; whiskers indicate data points within 1.5 × IQR. Significant differences of elf18 or water treatment compared with flg22-treated *Arabidopsis* Col-0, as determined by Student's t test, are shown.

(E) FLS2 $C^{1132,1135}S$ mutants are blocked in flg22-mediated increases in S-acylation. S-acylation state is shown following 20 min 1 μM flg22 treatment relative to untreated *Arabidopsis* plants of the same genotype (black, dashed line). Box plot shows median and IQR; whiskers indicate data points within 1.5 × IQR. Significant difference of each line compared with flg22-treated Col-0, as determined by Student's t test, are shown.

See also Figures S2 and S4.

FLS2 undergoes ligand-responsive S-acylation

We recently discovered that all plant RKs appear to be post-translationally modified by S-acylation.[27] FLS2 juxta-transmembrane domain cysteines (Cys830,831) are constitutively S-acylated but, surprisingly, S-acylation at these sites is dispensable for function.[27] All RK superfamily members subsequently tested, with or without an S-acylation site equivalent to FLS2 Cys830,831, also appear to be S-acylated.[27] This indicates that non-juxta-transmembrane S-acylation sites exist in RKs. Other post-translational modifications affecting FLS2, including phosphorylation,[28] ubiquitination[2] and SUMOylation,[1] are all responsive to ligand binding. Given the dynamic nature of S-acylation[24] we determined whether the FLS2 S-acylation state is also ligand responsive. In Col-0 wild-type plants, FLS2 S-acylation increased significantly following 20-min exposure to the FLS2 agonist peptide flg22. FLS2 S-acylation subsequently returned to basal levels within 1 h (Figures 1A and 1B). Consistent with ligand dependency, FLS2 S-acylation was contingent upon the FLS2 co-receptor BAK1 (Figure 1C). PLANT U-BOX12/13 (PUB12/13) are ubiquitin ligases proposed to promote FLS2 endocytosis and attenuate signaling.[2] FLS2 S-acylation is impaired in the *pub12/13* double mutant, suggesting that PUB12/13 action may be required for S-acylation to occur. In contrast, flg22-induced S-acylation of FLS2 was unaffected in CLATHRIN HEAVY CHAIN 2 (*chc2-1*) mutants[20] (Figure 1C). These data indicate that FLS2 S-acylation occurs after the initiation of signaling and the hypothesized ubiquitination thought to mark FLS2 for internalization, but before endocytosis of FLS2. Treatment of *Arabidopsis* Col-0 plants with elf18, an immunogenic peptide derived from bacterial elongation factor Tu, recognized by the RK ELONGATION FACTOR-Tu RECEPTOR (EFR),[5] failed to elevate FLS2 S-acylation (Figure 1D). This demonstrates that the increase in FLS2 S-acylation is specifically linked to the activation of FLS2 signaling and not a general phenomenon related to the activation of RK-mediated defense responses.

flg22 responsive S-acylation sites of FLS2 are located in the kinase domain C terminus and are conserved across the wider plant RK superfamily

FLS2 $C^{830,831}S$ mutants[27] lacking juxta-transmembrane S-acylation retain the ability to be S-acylated in response to flg22 (Figure S1A). FLS2 therefore contains additional S-acylation sites that are responsive to ligand perception. While FLS2 $C^{830,831}S$ expressed at native levels in unstimulated *Arabidopsis* is weakly S-acylated[27] (Figure S1A, untreated), we observed S-acylation of FLS2 $C^{830,831}S$ in the absence of flg22 when overexpressed in *Nicotiana benthamiana*. Mutation of FLS2 Cys1132 and 1135 in

Please cite this article in press as: Hurst et al., S-acylation stabilizes ligand-induced receptor kinase complex formation during plant pattern-triggered immune signaling, Current Biology (2023), https://doi.org/10.1016/j.cub.2023.02.065

CellPress

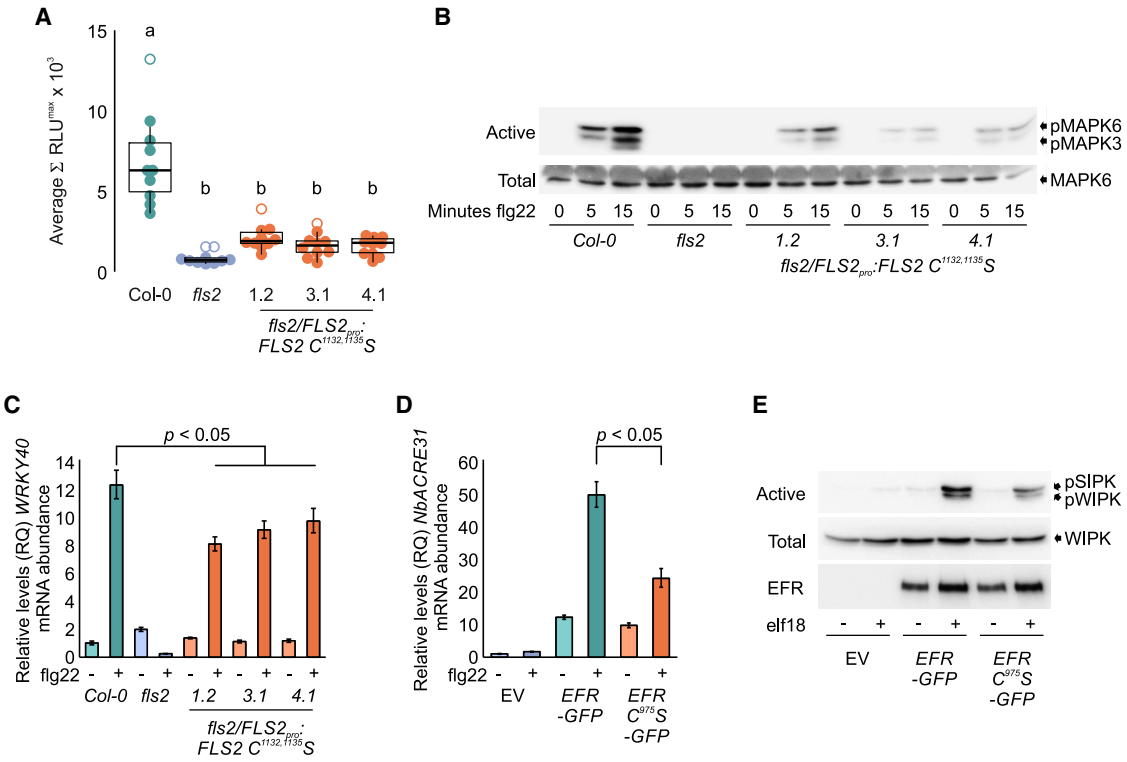

Figure 2. Acute responses to bacterial elicitor perception are reduced in FLS2 $C^{1132,1135}S$ and EFR-$C^{975}S$-expressing plants

(A) ROS production induced by 100 nM flg22 treatment of *Arabidopsis* seedlings. Data points are the sum of the 3 highest consecutive readings per sample. n = 10 per genotype. Statistical outliers are shown as open circles. Box shows median and IQR; whiskers show ±1.5 × IQR. Statistically significant differences at $p < 0.01$ are indicated (a and b) and were calculated using ANOVA and Tukey's HSD test.

(B) MAPK activation in *fls2/FLS2pro:FLS2* $C^{1132,1135}S$ *Arabidopsis* seedlings in response to 100 nM flg22, as determined over time by immunoblot analysis. pMAPK6/pMAPK3 show levels of active form of each MAPK. MAPK6 indicates total levels of MAPK6 as a loading control. Upper shadow band in MAPK6 blot is RuBisCO, detected non-specifically by secondary antibody.

(C) *WRKY40* mRNA abundance after 1 h treatment with 1 μM flg22 in fls2/FLS2pro:FLS2 $C^{1132,1135}S$ *Arabidopsis* seedlings, as determined by qRT-PCR. Values were calculated using the $\Delta\Delta_{CT}$ method, error bars represent RQMIN and RQMAX and constitute the acceptable error level for a 95% confidence interval, according to Student's t test.

(D) *NbACRE31* mRNA abundance after 3 h treatment with 1 μM elf18 in EFR-GFP and EFR $C^{975}S$-GFP-expressing *N. benthamiana* plants as determined by qRT-PCR. Values were calculated using the $\Delta\Delta_{CT}$ method, error bars represent RQMIN and RQMAX and constitute the acceptable error level for a 95% confidence interval, according to Student's t test.

(E) MAPK activation in EFR-GFP and EFR $C^{975}S$-GFP-expressing *N. benthamiana* plants in response to 15 min treatment with 1 μM elf18, as determined by immunoblot analysis. pSIPK/pWIPK show levels of active form of each MAPK. WIPK indicates total levels of WIPK as a loading control. EFR-GFP and EFR $C^{975}S$-GFP levels are shown as a control for dosage effects on MAPK activation.

See also Figure S1.

addition to Cys830 and 831 (FLS2 $C^{830,831,1132,1135}S$) abolished FLS2 S-acylation (Figure S1B) when overexpressed in *N. benthamiana*. Following this observation, we found that *fls2c/proFLS2:FLS2* $C^{1132,1135}S$ *Arabidopsis* plants (Figure S1C) showed no increase in S-acylation following flg22 treatment (Figure 1E), indicating that these cysteines are sites of ligand inducible S-acylation. Interestingly, 1–2 conserved cysteine residues at the kinase domain C terminus, corresponding to FLS2 Cys1132 and/or 1135, are found across all RKs in *Arabidopsis* and in RKs from basal Streptophyte Charophycean algae[29] (Figure S2), suggesting an evolutionarily conserved role for these cysteines. In support of this hypothesis, EFR-GFP[30] transiently expressed in *N. benthamiana* undergoes an elf18-induced increase in S-acylation that is blocked by the mutation of EFR Cys975, the cysteine homologous to FLS2 Cys1135 (Figures S1D, S1E, and S2).

RK C-terminal S-acylation is required for early immune signaling

Consistent with the conserved nature of the kinase domain cysteines among RKs, mutation of these cysteines affects FLS2 function. *fls2c/proFLS2:FLS2* $C^{1132,1135}S$ plants are impaired in several aspects of early immune signaling, such as reactive oxygen species production, MAP kinase activation and immune gene expression (Figures 2A–2C). In the absence of the flg22 ligand, both FLS2-3xMyc-GFP and FLS2 $C^{1132,1135}S$-3xMyc-GFP show a similar accumulation at the plasma membrane (Figure S3A; water treatments) and similar lateral membrane mobility (Figures S3B and S3C; water treatments). Remorins are cluster forming plasma membrane proteins proposed as markers for membrane nanodomains.[31] Specifically, REM1.3 (Remorin 1.3) nanodomains have a strong spatial overlap with FLS2

Please cite this article in press as: Hurst et al., S-acylation stabilizes ligand-induced receptor kinase complex formation during plant pattern-triggered immune signaling, Current Biology (2023), https://doi.org/10.1016/j.cub.2023.02.065

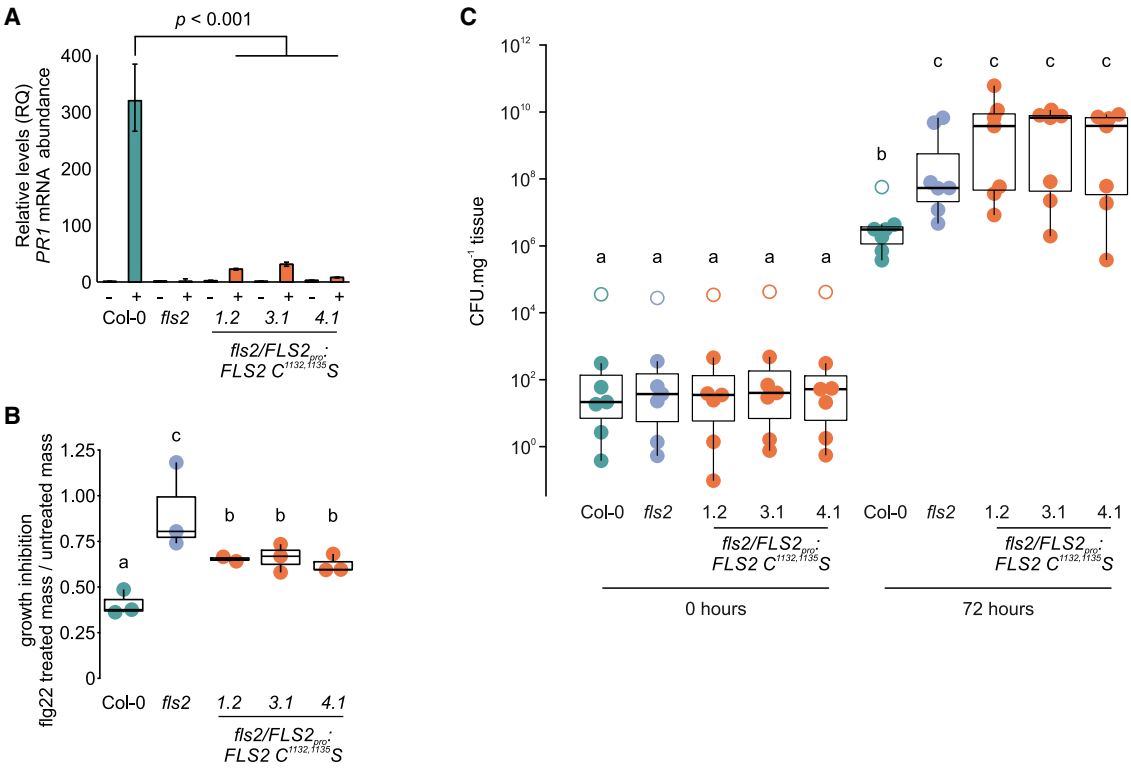

Figure 3. FLS2 S-acylation is required for long-term immune response outputs

(A) Induction of *PR1* gene expression after 24-h treatment with 1 mM flg22 in *fls2/FLS2pro:FLS2* $C^{1132,1135}S$ seedlings as determined by qRT-PCR. Values were calculated using the $\Delta\Delta_{CT}$ method, error bars represent RQMIN and RQMAX and constitute the acceptable error level for a 95% confidence interval, according to Student's t test. Significant differences in transcript mRNA detected in *fls2/FLS2pro:FLS2* $C^{1132,1135}S$ *Arabidopsis* seedlings compared with Col-0 levels in flg22-treated samples are indicated. Similar data were obtained over 3 biological repeats.

(B) Inhibition of growth after 10 days of 1 μM flg22 treatment is reduced in *fls2/FLS2pro:FLS2* $C^{1132,1135}S$ *Arabidopsis* seedlings. Box and whisker plots show data from 7 biological repeats (box denotes median and IQR, whiskers show ±1.5 × IQR), significant differences at $p < 0.01$ are indicated (a, b, and c) and calculated by ANOVA with Tukey HSD test.

(C) Resistance to *P. syringae* pv. tomato DC3000 infection is impaired by loss of FLS2 S-acylation in *fls2/FLS2pro:FLS2* $C^{1132,1135}S$ *Arabidopsis* plants. Box and whisker plots show data from 7 biological repeats (box denotes median and IQR, whiskers show ±1.5 × IQR, outliers are shown as open circles), significant differences at $p < 0.05$ are indicated (a, b, and c) and calculated by ANOVA with Tukey HSD test.

nanodomains.[32] Both FLS2-3xMyc-GFP and FLS2 $C^{1132,1135}$S-3xMyc-GFP show similar co-localization with REM1.3 nanodomains (Figures S3D–S3F). These data indicate that there is no aberrant basal behavior of the FLS2 $C^{1132,1135}$S mutant when compared with FLS2, which could account for the reduced response to flg22. To determine whether the conserved C-terminal cysteines may have a general role in RK function, we transiently expressed EFR-GFP[30] and EFR C^{975}S-GFP in *N. benthamiana*. elf18-induced MAP kinase phosphorylation, and immune gene induction was reduced in EFR C^{975}S-GFP expressing plants compared with EFR-GFP (Figures 2D and 2E), demonstrating that mutation of the conserved C-terminal cysteine in FLS2 and EFR has similar effects on early outputs, indicating a conserved mode of action. Structural homology modeling of FLS2 indicates that the $C^{1132,1135}$S mutation does not affect FLS2 kinase domain structure (Figure S4). Kinase activity is also dispensable for signaling by EFR.[33] The observed effects of the FLS2 $C^{1132,1135}$S and EFR C^{975}S mutations on signaling, therefore, cannot be explained through deleterious effects on kinase activity or structure.

FLS2 kinase domain S-acylation is required for late immune responses and anti-bacterial immunity

Early signaling outputs resulting from bacterial perception by FLS2 lead to longer term sustained responses to promote immunity. In line with decreased early immune responses, later flg22-induced gene expression, such as PATHOGENESIS-RELATED GENE 1 (*PR1*) expression, and seedling growth inhibition were affected in *fls2c/proFLS2:FLS2* $C^{1132,1135}S$ plants (Figures 3A and 3B). As a result of these cumulative signaling defects, FLS2 $C^{1132,1135}$S failed to complement *fls2c* mutant hyper-susceptibility to the pathogenic bacterium *Pseudomonas syringae* pv. tomato (*Pto*) DC3000 (Figure 3C).

S-acylation of FLS2 stabilizes flg22-induced FLS2-BAK1 signaling complexes within the plasma membrane

Differential solubility in cold non-ionic detergents such as Triton X-100 or IGEPAL CA-630, leading to the formation of detergent-soluble or -resistant membrane fractions (DSM and DRM, respectively), has been used to characterize changes to physical protein properties, particularly in the context of protein S-acylation.[22,34] *fls2c/proFLS2:FLS2* and *fls2c/proFLS2:FLS2* $C^{1132,1135}S$ plants

Please cite this article in press as: Hurst et al., S-acylation stabilizes ligand-induced receptor kinase complex formation during plant pattern-triggered immune signaling, Current Biology (2023), https://doi.org/10.1016/j.cub.2023.02.065

CellPress

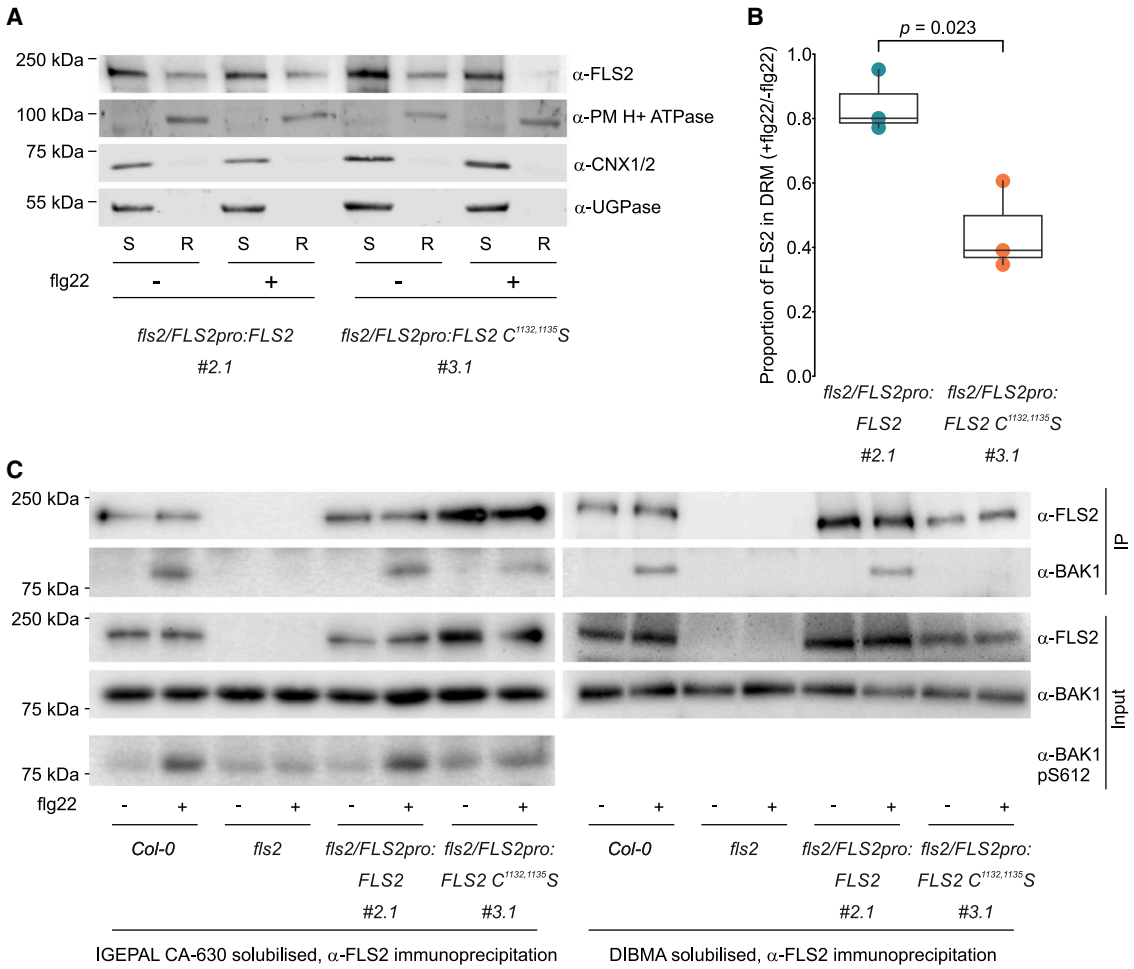

Figure 4. FLS2 $C^{1132,1135}S$ shows reduced interaction with BAK1 following flg22 stimulation

(A) FLS2 $C^{1132,1135}S$ shown altered DRM partitioning compared with FLS2. *Arabidopsis* flg22-treated seedlings were lysed in cold IGEPAL CA-630 buffer and separated into detergent-soluble (S) and detergent-resistant (R) fractions. Relative partitioning of FLS2 into each fraction was determined by western blotting with anti-FLS2 rabbit polyclonal antibody. Purity of fractions is shown by western blot using anti-PM H+ ATPase (PM ATPase, DRM marker), anti-Calnexin1/2 (CNX1/2, DSM marker), and anti-UDP-glucose pyrophosphorylase (UGPase, cytosol marker) antibodies.

(B) Quantification of FLS2 data shown in (A) from 3 biological repeats. Box plot shows median and IQR; whiskers indicate data points within 1.5 × IQR. Significance was calculated using Student's t test.

(C) FLS2 was immunoprecipitated from IGEPAL CA-630 (left) or DIBMA (right) solubilized flg22-treated *Arabidopsis* seedling lysates using anti-FLS2 rabbit polyclonal antibody. BAK1 recovery was assessed using rabbit polyclonal anti-BAK1 antibody. flg22-induced BAK1 autophosphorylation at Ser612 was assessed in IGEPAL CA-630 solubilized input samples using rabbit polyclonal anti-BAK1 pS612 antibody.

See also Figures S3 and S4.

were treated with or without flg22 and total cold IGEPAL CA-630 protein extracts were separated into DRM and DSM/cytosol fractions.[35] Following flg22 treatment, FLS2 abundance in DRMs showed a slight reduction, while FLS2 $C^{1132,1135}S$ DRM abundance decreased by ~50% (Figures 4A and 4B). Overall, these data suggest that the protein and/or lipid environment of the FLS2 $C^{1132,1135}S$-containing complex changes compared with wild type FLS2-containing complexes within 20 min of flg22 exposure.

Co-immunoprecipitation of flg22-induced FLS2-BAK1 complexes following solubilization with cold IGEPAL CA-630[36] indicated that FLS2-BAK1 interaction was reduced in FLS2 $C^{1132,1135}S$ mutants (Figure 4C). In support, flg22-induced BAK1 S^{612} auto-phosphorylation,[37] used as a marker of *in vivo* complex formation, was weaker in FLS2 $C^{1132,1135}S$-expressing plants (Figure 4C). In contrast to IGEPAL CA-630, diisobutylene/maleic acid (DIBMA) copolymer does not form DRM-like fractions. DIBMA disrupts lipid-lipid, but not protein-protein or protein-lipid, interactions to form membrane nanodiscs containing protein complexes within their membrane environment.[38] Co-immunoprecipitation of DIBMA-solubilized FLS2-BAK1 and FLS2 $C^{1132,1135}S$-BAK1 complexes after 20 min of flg22 treatment (Figure 4C) indicates that FLS2-BAK1 interactions are likely stabilized by protein-protein and protein-lipid interactions that are reduced or absent from FLS2 $C^{1132,1135}S$-BAK1 complexes.

Examination of FLS2 mobility by variable angle-total internal reflection fluorescence (VA-TIRF) microscopy (Figures S3B and S3C) shows no detectable change in FLS2-3xMyc-GFP or

Please cite this article in press as: Hurst et al., S-acylation stabilizes ligand-induced receptor kinase complex formation during plant pattern-triggered immune signaling, Current Biology (2023), https://doi.org/10.1016/j.cub.2023.02.065

FLS2 $C^{1132,1135}$S-3xMyc-GFP motion within the plasma membrane following flg22 treatment. However, we observed a decrease in the number of particles of FLS2 $C^{1132,1135}$S-3xMyc-GFP, but not wild-type FLS2-3xMyc-GFP, at the plasma membrane following 20 min of flg22 treatment (Figures S3B and S3C), suggesting premature, accelerated, or inappropriate endocytosis of flg22-bound FLS2 $C^{1132,1135}$S-3xMyc-GFP. Altogether, our observations indicate that FLS2 S-acylation stabilizes FLS2-BAK1 association and maintains FLS2 in a signaling competent state at the plasma membrane.

DISCUSSION

FLS2, a prototypical RK, has previously been shown to be S-acylated at a pair of juxta-transmembrane domain cysteines (Cys830,831), but S-acylation at these sites is dispensable for function.[27] Here, we demonstrate that FLS2 is S-acylated at additional cysteine residues (Cys1132,1135) in a ligand-responsive manner and that this is required for efficient flg22-triggered signaling and resistance to *P. syringae* DC3000 bacterial infection. FLS2 S-acylation occurs within minutes of flg22 perception and requires the co-receptor BAK1 and the PUB12/13 ubiquitin ligases but does not require CHC2 function (Figure 1). We therefore propose that FLS2 S-acylation occurs as a result of FLS2 activation but precedes entry into the endocytic pathway. Supporting this hypothesis, preventing ligand-mediated FLS2 S-acylation from occurring by using *fls2c/proFLS2:FLS2* $C^{1132,1135}S$ plants reduces early signaling outputs, such as the phosphorylation of MAPK and the production of ROS (Figure 2), processes unimpaired in mutants affecting FLS2 endocytosis.[18,20] Indeed, our data (Figures S3B and S3C) suggests a model where FLS2 S-acylation delays endocytosis and stabilizes the FLS2-BAK1 complex at the plasma membrane, thereby helping to sustain signaling competence. This failure to sufficiently prolong signaling competence also explains the defects observed in *fls2c/proFLS2:FLS2* $C^{1132,1135}S$ plants, where subsequent signaling outputs, such as *PR1* induction, growth inhibition and, ultimately, resistance to pathogenic bacteria (Figure 3), are greatly impaired. Following activation, FLS2 is endocytosed and degraded, with new FLS2 being synthesized within approximately 1 h of initial flg22 perception.[39,40] Our observation that FLS2 S-acylation returns to near basal levels after 1 h correlates with reported timings of degradation and *de novo* FLS2 synthesis,[39] but at present, we cannot exclude an active process of FLS2 de-S-acylation prior to endocytosis.

Sequence analysis of RKs from across the Streptophyte lineages indicate that the S-acylation site identified here at the C terminus of the FLS2 kinase domain is conserved across plant RK families throughout evolutionary history (Figure S2). Assessment of the elongation-factor-Tu-perceiving RK EFR indicates that, similarly to FLS2, it undergoes ligand-responsive S-acylation at this conserved cysteine (Cys975). Mutation of this cysteine in EFR recapitulates the downstream signaling defects observed in S-acylation-defective FLS2. We therefore hypothesize that there is a conserved role for S-acylation at these sites in other plant RKs. Recently, the P2K1/DORN1/LecRK-I.9 RK was proposed to undergo de-S-acylation followed by re-S-acylation during immune responses.[41] However, the site proposed is unique to the LecRK family, being distinct in proposed function, location, sequence, and structure to the universally conserved cysteine identified here, which is also present in P2K1 but was not considered in the previous work. These data demonstrate that, in common with other post-translational modifications, S-acylation may affect multiple sites within an RK with differing effects on RK function (e.g., this work and Hurst et al.[27]). The position and effect of the S-acylation site identified here at the C terminus of the FLS2 and EFR kinase domains is highly conserved among plant RKs, and is also found in the closely related receptor-like cytoplasmic kinases (RLCKs) that act downstream of activated RKs. This opens up the exciting possibility that S-acylation at the conserved C-terminal kinase site may potentially regulate the function of all RKs (and RLCKs) across plants in a similar manner to FLS2 and EFR. However, this hypothesis awaits further empirical testing.

RK signaling is initiated by the binding of a ligand (e.g., flg22) to its receptor (e.g., FLS2), which then facilitates the binding of a co-receptor (e.g., BAK1/SERK3). While this constitutes the minimal ligand recognition complex, substantial evidence supports a far larger number of proteins being intimately associated with both unstimulated and activated receptors and co-receptors. Indeed, existing data indicate that during the process of activation, RKs recruit or eject specific proteins from their complexes,[16,21,42,43] but precise molecular mechanisms determining these changes are not known. Live cell imaging of unstimulated FLS2 and BAK1 indicates that the presence or absence of the RK FERONIA (FER) has marked effects on nanoscale organization and mobility of RKs in the plasma membrane. In addition, activation of the RK FER by its ligand RALF23 alters BAK1 organization and mobility.[44] This indicates that both complex composition and the activation state of individual components affects behavior of the whole complex. Changes in direct protein-protein interaction can be explained by allosteric effects. However, it is also possible that alteration of the immediate (annular) lipid environment composition, curvature, or structure, brought about by changes in the physical properties of the complex, would act to recruit or exclude proteins based on their solubility and packing in the membrane environment surrounding the complex. This is, in essence, one of the principles proposed to underlie the formation of membrane nanodomains.[45,46] Activation of FLS2 following flg22 perception has been reported to decrease overall plasma membrane fluidity and increase plasma membrane order,[47] while changing sterol abundance in the plasma membrane affects all stages of FLS2 signaling.[48] This indicates that membrane composition and structure have profound effects on receptor complex function and supports the principle of protein-lipid interactions affecting or effecting RK function. S-acylation, a fatty-acid-based modification of proteins, has been shown to affect protein physical character and behavior in membrane environments.[34,49] S-acylation also affects membrane micro-curvature,[26] a key theoretical determinant of membrane component partitioning required for nanodomain formation.[45] We therefore hypothesize that FLS2 S-acylation modulates interactions between FLS2 and immune complex components and/or FLS2 proximal membrane lipid components and may effect changes in the composition of both. Altogether, our data support a model where flg22-induced, BAK1-dependent FLS2 S-acylation sustains FLS2-BAK1 association, prevents premature internalization of activated FLS2 complexes and, overall, acts to promote immune signaling.

STAR★METHODS

Detailed methods are provided in the online version of this paper and include the following:

- KEY RESOURCES TABLE
- RESOURCE AVAILABILITY
  - Lead contact
  - Materials availability
  - Data and code availability
- EXPERIMENTAL MODEL AND SUBJECT DETAILS
  - Plant lines and growth conditions
- METHOD DETAILS
  - Cloning and constructs
  - Eliciting peptides
  - Seedling growth inhibition
  - MAPK activation
  - Reactive oxygen species production
  - Gene expression analysis
  - Bacterial infection assays
  - Western blotting
  - S-acylation assays
  - Co-immunoprecipitation assays using IGEPAL CA-630
  - Co-immunoprecipitation assays using Diisobutylene-maleic acid (DIBMA)
  - Detergent resistant membrane preparation
  - Variable Angle - Total Internal Reflection Fluorescence (VA-TIRF) microscopy
  - Single particle tracking analysis
  - Co-localization analyses
  - Structural modelling of FLS2 kinase domain
- QUANTIFICATION AND STATISTICAL ANALYSIS

SUPPLEMENTAL INFORMATION

Supplemental information can be found online at https://doi.org/10.1016/j.cub.2023.02.065.

ACKNOWLEDGMENTS

We would like to thank Antje Heese and Paul Birch for critical discussions and advice during the preparation of this manuscript. Ari Sadanandom provided *P. syringae* pv. tomato DC3000. *bak1-4* seed was provided by Delphine Chinchilla, *chc2-1* seed by Antje Heese, and pub12/13 seed by Libo Shan. This work was supported by BBSRC EASTBIO-DTP studentship (grant number BB/M010996/1) to S.M. and P.A.H., BBSRC grants BB/M024911/1 and BB/P007902/1 to P.A.H., Royal Society grant RG140531 to P.A.H., a Heisenberg fellowship from the Deutsche Forschungsgemeinschaft to S.R., the Gatsby Charitable Foundation, the University of Zürich, the European Research Council (grant agreement 773153 IMMUNO-PEPTALK) to C.Z., the European Molecular Biology Organization (EMBO Long-Term Fellowship 438-2018), and the German Research Foundation (DFG grant CRC1101-A09) to J.G. S.J. was supported by the Scottish Government's Rural and Environment Science and Analytical Services Division (RESAS).

AUTHOR CONTRIBUTIONS

Conceptualization, C.H.H. and P.A.H. (lead); methodology, C.H.H., D.T., S.J., J.G., and P.A.H. (lead); software, S.J.; validation, C.H.H., D.T., S.M., and P.A.H.; formal analysis, C.H.H. (equal), K.X. (equal), J.G. (equal), and P.A.H. (lead); investigation, C.H.H. (lead), D.T. (equal), S.M., M.K., S.J., K.X., J.G. (equal), and P.A.H.; resources, S.R., C.Z., and P.A.H.; data curation, C.H.H. (equal), J.G. (equal), and P.A.H. (equal); writing – original draft, P.A.H. (lead); writing – review & editing, C.H.H., D.T., S.R., C.Z., J.G., and P.A.H. (lead); visualization, C.H.H., J.G., and P.A.H. (lead); supervision, S.R., C.Z., J.G., and P.A.H. (lead); project administration, P.A.H. (lead); funding acquisition, S.R. (equal), C.Z. (equal), J.G. (equal), and P.A.H. (equal).

DECLARATION OF INTERESTS

The authors declare no competing interests.

INCLUSION AND DIVERSITY

One or more of the authors of this paper self-identifies as a member of the LGBTQIA+ community.

Received: April 4, 2022
Revised: January 20, 2023
Accepted: February 21, 2023
Published: March 15, 2023

REFERENCES

1. Orosa, B., Yates, G., Verma, V., Srivastava, A.K., Srivastava, M., Campanaro, A., De Vega, D., Fernandes, A., Zhang, C., Lee, J., et al. (2018). SUMO conjugation to the pattern recognition receptor FLS2 triggers intracellular signaling in plant innate immunity. Nat. Commun. *9*, 5185.
2. Lu, D., Lin, W., Gao, X., Wu, S., Cheng, C., Avila, J., Heese, A., Devarenne, T.P., He, P., and Shan, L. (2011). Direct ubiquitination of pattern recognition receptor FLS2 attenuates plant innate immunity. Science *332*, 1439–1442.
3. Schulze, B., Mentzel, T., Jehle, A.K., Mueller, K., Beeler, S., Boller, T., Felix, G., and Chinchilla, D. (2010). Rapid heteromerization and phosphorylation of ligand-activated plant transmembrane receptors and their associated kinase BAK1. J. Biol. Chem. *285*, 9444–9451.
4. Zipfel, C., Robatzek, S., Navarro, L., Oakeley, E.J., Jones, J.D., Felix, G., and Boller, T. (2004). Bacterial disease resistance in Arabidopsis through flagellin perception. Nature *428*, 764–767.
5. Zipfel, C., Kunze, G., Chinchilla, D., Caniard, A., Jones, J.D., Boller, T., and Felix, G. (2006). Perception of the bacterial PAMP EF-Tu by the receptor EFR restricts Agrobacterium-mediated transformation. Cell *125*, 749–760.
6. Turnbull, D., and Hemsley, P.A. (2017). Fats and function: protein lipid modifications in plant cell signaling. Curr. Opin. Plant Biol. *40*, 63–70.
7. Shiu, S.H., and Bleecker, A.B. (2001). Receptor-like kinases from Arabidopsis form a monophyletic gene family related to animal receptor kinases. Proc. Natl. Acad. Sci. USA *98*, 10763–10768.
8. Shiu, S.H., and Bleecker, A.B. (2003). Expansion of the receptor-like kinase/Pelle gene family and receptor-like proteins in Arabidopsis. Plant Physiol. *132*, 530–543.
9. Divi, U.K., and Krishna, P. (2009). Brassinosteroid: a biotechnological target for enhancing crop yield and stress tolerance. N. Biotechnol. *26*, 131–136.
10. Lacombe, S., Rougon-Cardoso, A., Sherwood, E., Peeters, N., Dahlbeck, D., van Esse, H.P., Smoker, M., Rallapalli, G., Thomma, B.P., Staskawicz, B., et al. (2010). Interfamily transfer of a plant pattern-recognition receptor confers broad-spectrum bacterial resistance. Nat. Biotechnol. *28*, 365–369.
11. Gust, A.A., Brunner, F., and Nürnberger, T. (2010). Biotechnological concepts for improving plant innate immunity. Curr. Opin. Biotechnol. *21*, 204–210.
12. Marshall, A., Aalen, R.B., Audenaert, D., Beeckman, T., Broadley, M.R., Butenko, M.A., Caño-Delgado, A.I., de Vries, S., Dresselhaus, T., Felix, G., et al. (2012). Tackling drought stress: receptor-like kinases present new approaches. Plant Cell *24*, 2262–2278.

13. Gómez-Gómez, L., and Boller, T. (2000). FLS2: an LRR receptor-like kinase involved in the perception of the bacterial elicitor flagellin in Arabidopsis. Mol. Cell *5*, 1003–1011.

14. Chinchilla, D., Zipfel, C., Robatzek, S., Kemmerling, B., Nürnberger, T., Jones, J.D., Felix, G., and Boller, T. (2007). A flagellin-induced complex of the receptor FLS2 and BAK1 initiates plant defense. Nature *448*, 497–500.

15. Heese, A., Hann, D.R., Gimenez-Ibanez, S., Jones, A.M., He, K., Li, J., Schroeder, J.I., Peck, S.C., and Rathjen, J.P. (2007). The receptor-like kinase SERK3/BAK1 is a central regulator of innate immunity in plants. Proc. Natl. Acad. Sci. USA *104*, 12217–12222.

16. Lu, D., Wu, S., Gao, X., Zhang, Y., Shan, L., and He, P. (2010). A receptor-like cytoplasmic kinase, BIK1, associates with a flagellin receptor complex to initiate plant innate immunity. Proc. Natl. Acad. Sci. USA *107*, 496–501.

17. Spallek, T., Beck, M., Ben Khaled, S., Salomon, S., Bourdais, G., Schellmann, S., and Robatzek, S. (2013). ESCRT-I mediates FLS2 endosomal sorting and plant immunity. PLoS Genet. *9*, e1004035.

18. Smith, J.M., Leslie, M.E., Robinson, S.J., Korasick, D.A., Zhang, T., Backues, S.K., Cornish, P.V., Koo, A.J., Bednarek, S.Y., and Heese, A. (2014). Loss of Arabidopsis thaliana dynamin-Related Protein 2B reveals separation of innate immune signaling pathways. PLoS Pathog. *10*, e1004578.

19. Kadota, Y., Sklenar, J., Derbyshire, P., Stransfeld, L., Asai, S., Ntoukakis, V., Jones, J.D., Shirasu, K., Menke, F., Jones, A., et al. (2014). Direct regulation of the NADPH oxidase RBOHD by the PRR-associated kinase BIK1 during plant immunity. Mol. Cell *54*, 43–55.

20. Mbengue, M., Bourdais, G., Gervasi, F., Beck, M., Zhou, J., Spallek, T., Bartels, S., Boller, T., Ueda, T., Kuhn, H., et al. (2016). Clathrin-dependent endocytosis is required for immunity mediated by pattern recognition receptor kinases. Proc. Natl. Acad. Sci. USA *113*, 11034–11039.

21. Stegmann, M., Monaghan, J., Smakowska-Luzan, E., Rovenich, H., Lehner, A., Holton, N., Belkhadir, Y., and Zipfel, C. (2017). The receptor kinase FER is a RALF-regulated scaffold controlling plant immune signaling. Science *355*, 287–289.

22. Keinath, N.F., Kierszniowska, S., Lorek, J., Bourdais, G., Kessler, S.A., Shimosato-Asano, H., Grossniklaus, U., Schulze, W.X., Robatzek, S., and Panstruga, R. (2010). PAMP-induced changes in plasma membrane compartmentalization reveal novel components of plant immunity. J. Biol. Chem. *285*, 39140–39149.

23. Hemsley, P.A., Kemp, A.C., and Grierson, C.S. (2005). The TIP GROWTH DEFECTIVE1 S-acyl transferase regulates plant cell growth in Arabidopsis. Plant Cell *17*, 2554–2563.

24. Martin, B.R., Wang, C., Adibekian, A., Tully, S.E., and Cravatt, B.F. (2011). Global profiling of dynamic protein palmitoylation. Nat. Methods *9*, 84–89.

25. Hurst, C.H., and Hemsley, P.A. (2015). Current perspective on protein S-acylation in plants: more than just a fatty anchor? J. Exp. Bot. *66*, 1599–1606.

26. Mesquita, F.S., Abrami, L., Sergeeva, O., Turelli, P., Qing, E., Kunz, B., Raclot, C., Paz Montoya, J., Abriata, L.A., Gallagher, T., et al. (2021). S-acylation controls SARS-CoV-2 membrane lipid organization and enhances infectivity. Dev. Cell *56*, 2790–2807.e8.

27. Hurst, C.H., Wright, K.M., Turnbull, D., Leslie, K., Jones, S., and Hemsley, P.A. (2019). Juxta-membrane S-acylation of plant receptor-like kinases is likely fortuitous and does not necessarily impact upon function. Sci. Rep. *9*, 12818.

28. Wang, Y., Li, Z., Liu, D., Xu, J., Wei, X., Yan, L., Yang, C., Lou, Z., and Shui, W. (2014). Assessment of BAK1 activity in different plant receptor-like kinase complexes by quantitative profiling of phosphorylation patterns. J. Proteomics *108*, 484–493.

29. Gong, Z., and Han, G.Z. (2021). Flourishing in water: the early evolution and diversification of plant receptor-like kinases. Plant J. *106*, 174–184.

30. Holton, N., Nekrasov, V., Ronald, P.C., and Zipfel, C. (2015). The phylogenetically-related pattern recognition receptors EFR and XA21 recruit similar immune signaling components in monocots and dicots. PLoS Pathog. *11*, e1004602.

31. Jarsch, I.K., Konrad, S.S., Stratil, T.F., Urbanus, S.L., Szymanski, W., Braun, P., Braun, K.H., and Ott, T. (2014). Plasma membranes are subcompartmentalized into a plethora of coexisting and diverse microdomains in Arabidopsis and Nicotiana benthamiana. Plant Cell *26*, 1698–1711.

32. Bücherl, C.A., Jarsch, I.K., Schudoma, C., Segonzac, C., Mbengue, M., Robatzek, S., MacLean, D., Ott, T., and Zipfel, C. (2017). Plant immune and growth receptors share common signaling components but localise to distinct plasma membrane nanodomains. eLife *6*, e25114.

33. Bender, K.W., Couto, D., Kadota, Y., Macho, A.P., Sklenar, J., Derbyshire, P., Bjornson, M., DeFalco, T.A., Petriello, A., Font Farre, M., et al. (2021). Activation loop phosphorylation of a non-RD receptor kinase initiates plant innate immune signaling. Proc. Natl. Acad. Sci. USA *118*. e2108242118.

34. Abrami, L., Leppla, S.H., and van der Goot, F.G. (2006). Receptor palmitoylation and ubiquitination regulate anthrax toxin endocytosis. J. Cell Biol. *172*, 309–320.

35. Brown, D.A. (2002). Isolation and use of rafts. Curr. Protoc. Immunol. *Chapter 11*, Unit11.

36. Roux, M., Schwessinger, B., Albrecht, C., Chinchilla, D., Jones, A., Holton, N., Malinovsky, F.G., Tör, M., de Vries, S., and Zipfel, C. (2011). The Arabidopsis leucine-rich repeat receptor-like kinases BAK1/SERK3 and BKK1/SERK4 are required for innate immunity to hemibiotrophic and biotrophic pathogens. Plant Cell *23*, 2440–2455.

37. Perraki, A., DeFalco, T.A., Derbyshire, P., Avila, J., Séré, D., Sklenar, J., Qi, X., Stransfeld, L., Schwessinger, B., Kadota, Y., et al. (2018). Phosphocode-dependent functional dichotomy of a common co-receptor in plant signaling. Nature *561*, 248–252.

38. Oluwole, A.O., Danielczak, B., Meister, A., Babalola, J.O., Vargas, C., and Keller, S. (2017). Solubilization of membrane proteins into functional lipid-bilayer nanodiscs using a diisobutylene/maleic acid copolymer. Angew. Chem. Int. Ed. Engl. *56*, 1919–1924.

39. Smith, J.M., Salamango, D.J., Leslie, M.E., Collins, C.A., and Heese, A. (2014). Sensitivity to Flg22 is modulated by ligand-induced degradation and de novo synthesis of the endogenous flagellin-receptor FLAGELLIN-SENSING2. Plant Physiol. *164*, 440–454.

40. Robatzek, S., Chinchilla, D., and Boller, T. (2006). Ligand-induced endocytosis of the pattern recognition receptor FLS2 in Arabidopsis. Genes Dev. *20*, 537–542.

41. Chen, D., Hao, F., Mu, H., Ahsan, N., Thelen, J.J., and Stacey, G. (2021). S-acylation of P2K1 mediates extracellular ATP-induced immune signaling in Arabidopsis. Nat. Commun. *12*, 2750.

42. Yeh, Y.H., Panzeri, D., Kadota, Y., Huang, Y.C., Huang, P.Y., Tao, C.N., Roux, M., Chien, H.C., Chin, T.C., Chu, P.W., et al. (2016). The Arabidopsis malectin-like/LRR-RLK IOS1 is critical for BAK1-dependent and BAK1-independent pattern-triggered immunity. Plant Cell *28*, 1701–1721.

43. Imkampe, J., Halter, T., Huang, S., Schulze, S., Mazzotta, S., Schmidt, N., Manstretta, R., Postel, S., Wierzba, M., Yang, Y., et al. (2017). The Arabidopsis leucine-rich repeat receptor kinase BIR3 negatively regulates BAK1 receptor complex formation and stabilizes BAK1. Plant Cell *29*, 2285–2303.

44. Gronnier, J., Franck, C.M., Stegmann, M., DeFalco, T.A., Abarca, A., von Arx, M., Dünser, K., Lin, W., Yang, Z., Kleine-Vehn, J., et al. (2022). Regulation of immune receptor kinase plasma membrane nanoscale organization by a plant peptide hormone and its receptors. eLife *11*, e74162.

45. Allender, D.W., Giang, H., and Schick, M. (2020). Model plasma membrane exhibits a microemulsion in both leaves providing a foundation for "rafts". Biophys. J. *118*, 1019–1031.

46. Mamode Cassim, A., Gouguet, P., Gronnier, J., Laurent, N., Germain, V., Grison, M., Boutté, Y., Gerbeau-Pissot, P., Simon-Plas, F., and Mongrand, S. (2019). Plant lipids: key players of plasma membrane organization and function. Prog. Lipid Res. *73*, 1–27.

47. Sandor, R., Der, C., Grosjean, K., Anca, I., Noirot, E., Leborgne-Castel, N., Lochman, J., Simon-Plas, F., and Gerbeau-Pissot, P. (2016). Plasma membrane order and fluidity are diversely triggered by elicitors of plant defense. J. Exp. Bot. *67*, 5173–5185.

48. Cui, Y., Li, X., Yu, M., Li, R., Fan, L., Zhu, Y., and Lin, J. (2018). Sterols regulate endocytic pathways during flg22-induced defense responses in Arabidopsis. Development *145*, dev165688.

49. Blaskovic, S., Blanc, M., and van der Goot, F.G. (2013). What does S-palmitoylation do to membrane proteins? FEBS J. *280*, 2766–2774.

50. Hurst, C.H., Turnbull, D., Myles, S.M., Leslie, K., Keinath, N.F., and Hemsley, P.A. (2018). Variable effects of C-terminal fusions on FLS2 function: not all epitope tags are created equal. Plant Physiol. *177*, 522–531.

51. Koncz, C., and Schell, J. (1986). The promoter of TL-DNA gene 5 controls the tissue-specific expression of chimaeric genes carried by a novel type of Agrobacterium binary vector. Molec. Gen. Genet. *204*, 383–396.

52. Ishiga, Y., Ishiga, T., Uppalapati, S.R., and Mysore, K.S. (2011). Arabidopsis seedling flood-inoculation technique: a rapid and reliable assay for studying plant-bacterial interactions. Plant Methods *7*, 32.

53. Kemmerling, B., Schwedt, A., Rodriguez, P., Mazzotta, S., Frank, M., Qamar, S.A., Mengiste, T., Betsuyaku, S., Parker, J.E., Müssig, C., et al. (2007). The BRI1-associated kinase 1, BAK1, has a brassinolide-independent role in plant cell-death control. Curr. Biol. *17*, 1116–1122.

54. Schindelin, J., Arganda-Carreras, I., Frise, E., Kaynig, V., Longair, M., Pietzsch, T., Preibisch, S., Rueden, C., Saalfeld, S., Schmid, B., et al. (2012). Fiji: an open-source platform for biological-image analysis. Nat. Methods *9*, 676–682.

55. Ershov, D., Phan, M.S., Pylvänäinen, J.W., Rigaud, S.U., Le Blanc, L., Charles-Orszag, A., Conway, J.R.W., Laine, R.F., Roy, N.H., Bonazzi, D., et al. (2022). TrackMate 7: integrating state-of-the-art segmentation algorithms into tracking pipelines. Nat. Methods *19*, 829–832.

56. Parutto, P., Heck, J., Lu, M., Kaminski, C., Avezov, E., Heine, M., and Holcman, D. (2022). High-throughput super-resolution single-particle trajectory analysis reconstructs organelle dynamics and membrane reorganization. Cell Rep. Methods *2*, 100277.

57. R Core Team (2022). R: A Language and Environment for Statistical Computing (R Foundation for Statistical Computing).

58. RStudio Team (2020). RStudio: Integrated Development for R (RStudio, PBC).

59. Clough, S.J., and Bent, A.F. (1998). Floral dip: a simplified method for Agrobacterium-mediated transformation of Arabidopsis thaliana. Plant J. *16*, 735–743.

60. Turnbull, D., Yang, L., Naqvi, S., Breen, S., Welsh, L., Stephens, J., Morris, J., Boevink, P.C., Hedley, P.E., Zhan, J., et al. (2017). RXLR effector AVR2 up-regulates a brassinosteroid-responsive bHLH transcription factor to suppress immunity. Plant Physiol. *174*, 356–369.

61. Karimi, M., Inzé, D., and Depicker, A. (2002). Gateway vectors for Agrobacterium-mediated plant transformation. Trends Plant Sci. *7*, 193–195.

62. Schwessinger, B., Roux, M., Kadota, Y., Ntoukakis, V., Sklenar, J., Jones, A., and Zipfel, C. (2011). Phosphorylation-dependent differential regulation of plant growth, cell death, and innate immunity by the regulatory receptor-like kinase BAK1. PLoS Genet. *7*, e1002046.

63. Mersmann, S., Bourdais, G., Rietz, S., and Robatzek, S. (2010). Ethylene signaling regulates accumulation of the FLS2 receptor and is required for the oxidative burst contributing to plant immunity. Plant Physiol *154*, 391–400. https://doi.org/10.1104/pp.110.154567.

64. Wathugala, D.L., Hemsley, P.A., Moffat, C.S., Cremelie, P., Knight, M.R., and Knight, H. (2012). The Mediator subunit SFR6/MED16 controls defense gene expression mediated by salicylic acid and jasmonate responsive pathways. New Phytol. *195*, 217–230.

65. Schmittgen, T.D., and Livak, K.J. (2008). Analyzing real-time PCR data by the comparative C(T) method. Nat. Protoc. *3*, 1101–1108.

66. Hurst, C.H., Turnbull, D., Plain, F., Fuller, W., and Hemsley, P.A. (2017). Maleimide scavenging enhances determination of protein S-palmitoylation state in acyl-exchange methods. BioTechniques *62*, 69–75.

67. Gorinski, N., Wojciechowski, D., Guseva, D., Abdel Galil, D., Mueller, F.E., Wirth, A., Thiemann, S., Zeug, A., Schmidt, S., Zareba-Kozioł, M., et al. (2020). DHHC7-mediated palmitoylation of the accessory protein barttin critically regulates the functions of ClC-K chloride channels. J. Biol. Chem. *295*, 5970–5983.

68. Borner, G.H., Sherrier, D.J., Weimar, T., Michaelson, L.V., Hawkins, N.D., Macaskill, A., Napier, J.A., Beale, M.H., Lilley, K.S., and Dupree, P. (2005). Analysis of detergent-resistant membranes in Arabidopsis. Evidence for plasma membrane lipid rafts. Plant Physiol. *137*, 104–116.

69. Martz, F., Wilczynska, M., and Kleczkowski, L.A. (2002). Oligomerization status, with the monomer as active species, defines catalytic efficiency of UDP-glucose pyrophosphorylase. Biochem. J. *367*, 295–300.

70. Gronnier, J., Franck, C.M., Stegmann, M., DeFalco, T.A., Cifuentes, A.A., Dünser, K., Lin, W., Yang, Z., Kleine-Vehn, J., Ringli, C., et al. (2020). FERONIA regulates FLS2 plasma membrane nanoscale dynamics to modulate plant immune signaling. Preprint at bioRxiv. https://doi.org/10.1101/2020.07.20.212233.

71. Jaqaman, K., Loerke, D., Mettlen, M., Kuwata, H., Grinstein, S., Schmid, S.L., and Danuser, G. (2008). Robust single-particle tracking in live-cell time-lapse sequences. Nat. Methods *5*, 695–702.

72. Sage, D., Neumann, F.R., Hediger, F., Gasser, S.M., and Unser, M. (2005). Automatic tracking of individual fluorescence particles: application to the study of chromosome dynamics. IEEE Trans. Image Process. *14*, 1372–1383.

73. Bolte, S., and Cordelières, F.P. (2006). A guided tour into subcellular colocalization analysis in light microscopy. J. Microsc. *224*, 213–232.

74. Kelley, L.A., Mezulis, S., Yates, C.M., Wass, M.N., and Sternberg, M.J. (2015). The Phyre2 web portal for protein modeling, prediction and analysis. Nat. Protoc. *10*, 845–858.

75. Blaum, B.S., Mazzotta, S., Nöldeke, E.R., Halter, T., Madlung, J., Kemmerling, B., and Stehle, T. (2014). Structure of the pseudokinase domain of BIR2, a regulator of BAK1-mediated immune signaling in Arabidopsis. J. Struct. Biol. *186*, 112–121.

76. Ittisoponpisan, S., Islam, S.A., Khanna, T., Alhuzimi, E., David, A., and Sternberg, M.J.E. (2019). Can predicted protein 3D structures provide reliable insights into whether missense variants are disease associated? J. Mol. Biol. *431*, 2197–2212.

Please cite this article in press as: Hurst et al., S-acylation stabilizes ligand-induced receptor kinase complex formation during plant pattern-triggered immune signaling, Current Biology (2023), https://doi.org/10.1016/j.cub.2023.02.065

STAR★METHODS

KEY RESOURCES TABLE

REAGENT or RESOURCE	SOURCE	IDENTIFIER
Antibodies		
Anti-FLS2 (rabbit polyclonal)	Piers Hemsley[50]	non-commercial
Anti-BAK1 (rabbit polyclonal)	Agrisera	Cat# AS12 1858; RRID: AB_2884902
Anti-FLS2 (rabbit polyclonal)	Cyril Zipfel[14]	non-commercial
Anti-BAK1 (rabbit polyclonal)	Cyril Zipfel[36]	non-commercial
Anti-BAK1 pSer612 (rabbit polyclonal)	Cyril Zipfel[37]	non-commercial
Anti-Calnexin1/2 (rabbit polyclonal)	Agrisera	Cat# AS12 2365
Anti-PM H+ ATPase (chicken polyclonal)	Agrisera	Cat# AS13 2671
Anti-UGPase (rabbit polyclonal)	Agrisera	Cat# AS05 086; RRID: AB_1031827
Anti-p44/42 MAPK (Erk1/2) (rabbit polyclonal)	Cell Signalling Technology	Cat# 9102; RRID: AB_330744
Anti-MAPK6 (Arabidopsis) (rabbit polyclonal)	Merck	Cat# A7104; RRID: AB_476760
Anti-GFP (mouse monoclonal IgG1κ clones 7.1 and 13.1)	Roche	Cat# 11814460001; RRID: AB_390913
Anti-Rabbit HRP (goat polyclonal)	Pierce	Cat# 31460; RRID: AB_228341
anti-rabbit IgG-HRP Trueblot	Rockland	Cat# 18-8816-31; RRID: AB_2610847
anti-rabbit IgG (whole molecule)–HRP	Sigma	Cat# A0545; RRID: AB_257896
Clean-Blot HRP	ThermoFisher	Cat# 21230; RRID: AB_2864363
Anti-Rabbit IR Dye 800CW (goat polyclonal)	Licor	Cat# 926-32211; RRID: AB_621843
Anti-Mouse IR Dye 800CW (goat polyclonal)	Licor	Cat# 926-32210; RRID: AB_621842
Anti-Chicken IR Dye 800CW (donkey polyclonal)	Licor	Cat# 926-32218; RRID: AB_1850023
Bacterial and virus strains		
E. coli NEB 5-alpha	New England Biolabs	Cat# C2987U
Agrobacterium tumefaciens GV3101 (pMP90)	Koncz and Schell[51]	N/A
Pseudomonas syringae pv. tomato DC3000	Ari Sadanandom[52]	N/A
Chemicals, peptides, and recombinant proteins		
Flg22 (QRLSTGSRINSAKDDAAGLQIA)	Dundee Cell Products	synthesized
Flg22 (QRLSTGSRINSAKDDAAGLQIA)	EZBiolab	synthesized
Elf18 (Ac-SKEKFERTKPHVNVGTIG)	Peptide Protein Research	synthesized
Experimental models: Organisms/strains		
Arabidopsis thaliana Col-0 ecotype	NASC	Cat# N1093
fls2 mutant (*Arabidopsis thaliana* Col-0 ecotype)	Zipfel et al.[4]	N/A
bak1-4 mutant (*Arabidopsis thaliana* Col-0 ecotype)	Kemmerling et al.[53]	N/A
chc2-1 mutant (*Arabidopsis thaliana* Col-0 ecotype)	Mbengue et al.[20]	N/A
pub12/13 mutant (*Arabidopsis thaliana* Col-0 ecotype)	Lu et al.[2]	N/A
fls2/*FLS2*$_{pro}$:*FLS2* (*Arabidopsis thaliana* Col-0 ecotype)	Hurst et al.[50]	N/A

(*Continued on next page*)

Please cite this article in press as: Hurst et al., S-acylation stabilizes ligand-induced receptor kinase complex formation during plant pattern-triggered immune signaling, Current Biology (2023), https://doi.org/10.1016/j.cub.2023.02.065

CellPress

Continued

REAGENT or RESOURCE	SOURCE	IDENTIFIER
fls2/$FLS2_{pro}$:FLS2 $C^{830,831}S$ (*Arabidopsis thaliana* Col-0 ecotype)	Hurst et al.[27]	N/A
fls2/$FLS2_{pro}$:FLS2 $C^{1132,1135}S$ (*Arabidopsis thaliana* Col-0 ecotype)	This paper	N/A
Oligonucleotides		
PR1 qPCR F2	CATCCTGCATATGATGCTCCT	Sigma-Aldrich
PR1 qPCR R2	TCGTGGGAATTATGTGAACG	Sigma-Aldrich
PEX4 qPCR For	AGAATGCTTGGAGTCCTGCT	Sigma-Aldrich
PEX4 qPCR Rev	TGAACCCTCTCACATCACCA	Sigma-Aldrich
WRKY40 qPCR F	AGATCTCACTATTGGCGTTACTC	Sigma-Aldrich
WRKY40 qPCR R	GCATCTCCGAGAGCTTCTTG	Sigma-Aldrich
NbAcre31 qPCR For	AATTCGGCCATCGTGATCTTGGTC	Sigma-Aldrich
NbAcre31 qPCR Rev	GAGAAACTGGGATTGCCTGAAGGA	Sigma-Aldrich
EFR C975S For (site directed mutagenesis)	GGGGATAAAGtctTCTGAAGAATATC	Sigma-Aldrich
EFR C975S Rev (site directed mutagenesis)	ACCTGCAAAACCAGTCTC	Sigma-Aldrich
FLS2 C1132,1135S R (site directed mutagenesis)	ttcagtACAAGCTCTAGACCTGAAG	Sigma-Aldrich
FLS2 C1132,1135S F (site directed mutagenesis)	caaagaAAGCTTCAGAAAGT CTTCAATAG	Sigma-Aldrich
Recombinant DNA		
pENTR D-TOPO $FLS2_{pro}$:FLS	Hurst et al.[50]	N/A
pK7WG,0 $FLS2_{pro}$:FLS	Hurst et al.[50]	N/A
pK7WG,0 $FLS2_{pro}$:FLS2 $C^{830,831}S$	Hurst et al.[27]	N/A
pENTR D-TOPO $FLS2_{pro}$: FLS2 $C^{830,831,1132,1135}S$	This paper	N/A
pK7WG,0 $FLS2_{pro}$: FLS2 $C^{830,831,1132,1135}S$	This paper	N/A
pENTR D-TOPO $FLS2_{pro}$: FLS2 $C^{1132,1135}S$	This paper	N/A
pK7WG,0 $FLS2_{pro}$:FLS2 $C^{1132,1135}S$	This paper	N/A
pENTR D-TOPO $FLS2_{pro}$: FLS2-3xMYC-GFP	This paper	N/A
pK7WG,0 $FLS2_{pro}$:FLS2-3xMYC-GFP	This paper	N/A
pENTR D-TOPO $FLS2_{pro}$: FLS2 $C^{1132,1135}S$-3xMYC-GFP	This paper	N/A
pK7WG,0 $FLS2_{pro}$:FLS2 $C^{1132,1135}$ S-3xMYC-GFP	This paper	N/A
pEARLEYGATE100 $35S_{pro}$: EFR-GFP	Holton et al.[30]	N/A
pEARLEYGATE100 $35S_{pro}$: EFR $C^{975}S$-GFP	This paper	N/A
$35S_{pro}$:mRFP-REM1	Bücherl et al.[32]	N/A
Software and algorithms		
Fiji	Schindelin et al.[54]	https://imagej.net/software/fiji/downloads
TrackMate7	Ershov et al.[55]	https://imagej.net/plugins/trackmate/index
SPTAnalysis	Parutto et al.[56]	https://doi.org/10.5281/zenodo.6862643
R	R core team[57]	https://www.R-project.org/
RStudio	RStudio team[58]	https://posit.co/products/open-source/rstudio/

Please cite this article in press as: Hurst et al., S-acylation stabilizes ligand-induced receptor kinase complex formation during plant pattern-triggered immune signaling, Current Biology (2023), https://doi.org/10.1016/j.cub.2023.02.065

RESOURCE AVAILABILITY

Lead contact

Further information or requests for resources and reagents should be directed to and will be fulfilled by the lead contact, Piers Hemsley (pahemsley@dundee.ac.uk).

Materials availability

All novel materials described in this paper will be made available upon request, subject to completion of an MTA.

Data and code availability

- All data reported in this paper will be shared by the lead contact upon request.
- No original code is reported in this paper.
- Additional information required to reanalyze the data reported in this paper is available from the lead contact upon request.

EXPERIMENTAL MODEL AND SUBJECT DETAILS

Plant lines and growth conditions

All Arabidopsis lines were in the Col-0 accession background. The *fls2*,[4] *bak1-4*,[53] pub12/13[2] and *chc2-1*[20] mutants have all been described previously. Transgenic *fls2*/$FLS2_{pro}$:*FLS2* are already described[50] and *fls2*/$FLS2_{pro}$:*FLS2* $C^{1132,1135}S$ mutant variant lines were generated by Agrobacterium-mediated floral dip transformation.[59] T_3 homozygous plants were used for all experiments. Plant material for experiments was grown on 0.5x MS medium, 0.8% phytagar under 16:8 light:dark cycles at 20 °C in MLR-350 growth chambers (Panasonic). For transient expression *Nicotiana benthamiana* plants were grown in 16:8 light:dark cycles at 24 °C and used at 4-5 weeks old. *A. tumefaciens* GV3101 (pMP90) mediated transient expression was performed as described[60] using an OD600 of 0.1 of each expression construct alongside the p19 silencing suppressor at an OD600 of 0.1. Tissue was harvested 48-60 hours post infiltration.

METHOD DETAILS

Cloning and constructs

All *FLS2* mutant variants used in this study are based on fully functional $FLS2_{pro}$:*FLS2* construct able to complement *fls2* mutants[50] containing the described FLS2 promoter and open reading frame with stop codon.[4] All construct manipulations were performed on pENTR D-TOPO based vectors. Nucleotide changes were generated using Q5 site directed mutagenesis kit (NEB) according to the manufacturer's guidelines. $FLS2_{pro}$:*FLS2-3xMYC-EGFP* and $FLS2_{pro}$:*FLS2* $C^{1132,1135}S$-*3xMYC-EGFP* were made by recombinatorial cloning in yeast using a 3xMYC-EGFP PCR fragment amplified from $FLS2_{pro}$:*FLS2-3xMYC-EGFP*[40] recombined with pENTR D-TOPO $FLS2_{pro}$:*FLS2* or pENTR D-TOPO $FLS2_{pro}$:*FLS2* $C^{1132,1135}S$. Entry clones were recombined into pK7WG,0[61] using Gateway technology (ThermoFisher) to generate expression constructs. Expression constructs were transformed into *Agrobacterium tumefaciens* strain GV3101 (pMP90)[51] for transformation of either Arabidopsis or *Nicotiana benthamiana*.

Eliciting peptides

Flg22 peptide (QRLSTGSRINSAKDDAAGLQIA) was synthesized by Dundee Cell Products (Dundee, UK). Elf18 peptide (Ac-SKEKFERTKPHVNVGTIG) was synthesized by Peptide Protein Research (Bishops Waltham, UK).

Seedling growth inhibition

For each biological replicate four days post-germination, 10 seedlings of the named genotypes were transferred to 12-well plates (5 seedlings per well), ensuring the cotyledons were not submerged. Wells contained 2 mL of 0.5x MS liquid medium with or without 1 μM flg22. Seedlings were incubated for 10 days and the fresh weight of pooled seedlings in each genotype for each treatment measured and an average taken. Flg22- treated/untreated weights for each genotype were calculated and presented data is an average of these data over three biological repeats. Fully independent biological repeats were performed over a period of 6 months with each genotype only being present once in each repeat.

MAPK activation

Essentially as for Schwessinger et al.[62]; 6 Arabidopsis seedlings of each genotype 10 days post germination were treated with 100 nM flg22 for the indicated times in 2 mL 0.5x MS medium. The 6 seedlings from each genotype at each time point for each treatment were pooled before further analysis. Fully independent biological repeats were performed over a period of 2 years with each genotype only being present once in each repeat. To assess EFR induced MAPK activation in *N. benthamiana* leaves from 5-week-old plants were transiently transformed by agrobacterium infiltration (OD600 0.1 of each construct plus p19 at OD600

Please cite this article in press as: Hurst et al., S-acylation stabilizes ligand-induced receptor kinase complex formation during plant pattern-triggered immune signaling, Current Biology (2023), https://doi.org/10.1016/j.cub.2023.02.065

0.1). 60 hours after transformation, 1 μM elf18 peptide in water or water only was infiltrated into the leaf and samples harvested after 15 minutes. Samples were subsequently processed as described.[62]

Reactive oxygen species production

Protocol based on Mersmann et al.[63] Essentially, 10 seedlings of each genotype were grown for 14 days individually in 100 μL of 0.5x MS medium with 0.5% sucrose in 96-well plates (PerkinElmer). Conditions were maintained at 22 °C with 12:12 light:dark cycles. Growth medium was exchanged for water with 10 nM flg22 for 1 hour, before replacing with water for a further 1 hour. ROS burst was then induced by replacing with a solution containing 100 nM flg22, 400 nM luminol (Fluka), and 20 μg/mL peroxidase (Sigma). Luminescence in each well was measured every 2 minutes in a Varioskan Lux (Thermo Fisher) for 30 cycles (approx. 1 hour total).

Gene expression analysis

Ten seedlings of each genotype 10 days post-germination were treated with 1 μM flg22 or water for the indicated times. The 10 seedlings from each genotype/treatment at each time point for each treatment were pooled before further analysis. RNA was extracted using RNAeasy Plant kit with on column DNAse digestion according to the manufacturer's instructions (Qiagen). Two micrograms RNA was reverse transcribed using a High-Capacity cDNA Reverse Transcription kit (Applied Biosystems). All transcripts were amplified using validated gene-specific primers.[50] Expression levels were normalized against *PEX4* (At5g25760).[64] Each sample was analyses in triplicate (technical repeats) for each primer pair within each biological repeat. Relative quantification (RQ) was achieved using the $\Delta\Delta_{CT}$ (comparative cycle threshold) method.[65] Significant differences between samples were determined from a 95% confidence interval calculated using the t-distribution. Fully independent biological repeats were performed over a period of 2 years with each genotype only being present once in each repeat.

Bacterial infection assays

Infection assays of Arabidopsis lines by *Pseudomonas syringae* pv. tomato DC3000 were performed using seedling flood inoculation assays as described.[52]

Western blotting

FLS2 was detected using rabbit polyclonal antisera raised against the C-terminus of FLS2 as previously described.[15,66] Anti-p44/42 MAPK (Erk1/2) (Cell Signalling Technology #9102) was used to detect phosphorylated MAPK3/6 according to manufacturer's recommendations at 1:2000 dilution. Total Arabidopsis MAPK6 or *N. benthamiana* WIPK was detected using anti-Arabidopsis MPK6 (Sigma A7104) at 1:2000. Rabbit polyclonal antibodies against BAK1 were as described[36] or obtained from Agrisera (AS12 1858) and used at 1:5000 dilution. BAK1 phospho-S612 was detected using polyclonal rabbit antisera as described.[37] GFP was detected using mouse monoclonal antibodies (Roche 11814460001). Plasma membrane H+ ATPase (Agrisra AS13 2671), Calnexin 1/2 (Agrisera AS12 2365) and UDP-glucose pyrophosphorylase (Agrisera AS05 086) were all used at 1:2500. HRP (ECL) or fluorophore (Licor CLx) conjugated secondary antibodies were used to visualize antibody reacting proteins, and Clean-Blot HRP (Thermo Fisher) secondary antibody was used for immunoprecipitation experiments. ECL Western blots were developed using SuperSignal West pico and femto in a 3:1 ratio by volume and signal captured using a Syngene G:box storm imager and quantitative photon count data stored as Syngene SGD files. Signal intensity was quantified from SGD files using Syngene GeneTools software. Fluorescent western blots were imaged using a Licor CLx controlled by ImageStudio and quantified using Licor ImageStudio.

S-acylation assays

S-acylation assays using acyl-biotin exchange (ABE) were performed exactly as described.[66] For flg22-dependent changes in FLS2 S-acylation, 7 seedlings 10 days post germination were transferred to each well of 12-well plates. Each well contained 2 mL 0.5 x MS liquid medium. Seedling were incubated for 24 hours on an orbital mixer (Luckham R100/TW Rotatest Shaker, 38 mm orbit at 75 RPM). Thereafter, 100 μL of 0.5 x MS media containing flg22 was added to give a final flg22 concentration of 10 μM. Seedlings were incubated with continued mixing for the indicated times before harvesting. Relative S-acylation is calculated using: (EX+ intensity$^{\text{SAMPLE X}}$ / LC+ intensity$^{\text{SAMPLE X}}$) / (EX+ intensity$^{\text{REFERENCE SAMPLE}}$ / LC+ intensity $^{\text{REFERENCE SAMPLE}}$).[67] Sample X refers to the sample of interest, reference sample is typically untreated control plants.

Co-immunoprecipitation assays using IGEPAL CA-630

Seedlings grown on solid 0.5x MS for 30-35 days were transferred to wells of a 6-well plates and grown for 7 days in 0.5x MS 2 mM MES-KOH, pH 5.8. Thereafter, the seedlings were transferred in beakers containing 40 mL of 0.5x MS 2 mM MES-KOH, pH 5.8 and subsequently treated with sterile mQ water with or without flg22 (final concentration of 100 nM) and incubated for 10 minutes. The seedlings were then frozen in liquid nitrogen and proteins extracted in 50 mM Tris-HCl pH 7.5, 150 mM NaCl, 10% glycerol, 5 mM dithiothreitol, 1% protease inhibitor cocktail (Sigma Aldrich), 2 mM Na_2MoO_4, 2.5 mM NaF, 1.5 mM activated Na_3VO_4, 1 mM phenylmethanesulfonyl fluoride and 0.5% IGEPAL for 40 minutes at 4 °C. Lysates were clarified at 10,000 g for 20 minutes at 4 °C and the supernatants were filtered through miracloth. For immunoprecipitations, α-rabbit Trueblot agarose beads (eBioscience) coupled with α-FLS2 antibodies[14] were incubated with the crude extract for 3 hours at 4 °C. Subsequently, beads were washed 3 times (50 mM Tris-HCl pH 7.5, 150 mM NaCl, 1 mM phenylmethanesulfonyl fluoride, 0.1% IGEPAL) before adding Laemmli buffer and incubating for 10 minutes at 95 °C. Protein samples were separated in 10% bisacrylamide gels at 150 V for approximately 2 hours and

Please cite this article in press as: Hurst et al., S-acylation stabilizes ligand-induced receptor kinase complex formation during plant pattern-triggered immune signaling, Current Biology (2023), https://doi.org/10.1016/j.cub.2023.02.065

transferred into activated PVDF membranes at 100 V for 90 minutes. Immunoblotting was performed with antibodies diluted in blocking solution (5% fat-free milk in TBS with 0.1% (v/v) Tween-20). Antibodies used in this study: α-BAK1[36] (1:5000); α-FLS2[14] (1:1000); α-BAK1 pS612[37] (1:3000). Blots were developed with Pierce ECL/ ECL Femto Western Blotting Substrate (Thermo Scientific). The following secondary antibodies were used: anti-rabbit IgG-HRP Trueblot (Rockland, 18-8816-31, dilution 1:10000) for detection of FLS2-BAK1 co-immunoprecipitation or anti-rabbit IgG (whole molecule)–HRP (A0545, Sigma, dilution 1:10000) for all other western blots.

Co-immunoprecipitation assays using Diisobutylene-maleic acid (DIBMA)

For each genotype, 2 x 10 seedlings 10 days post-germination were transferred to each well of 12-well plate containing 2 mL 0.5 x MS liquid medium and incubated for 24 hours on an orbital mixer (Luckham R100/TW Rotatest Shaker, 38 mm orbit at 75 RPM). Thereafter, 100 μL of 0.5 x MS media containing flg22 was added to give a final flg22 concentration of 10 μM. The seedlings were further incubated with continued mixing for 20 minutes prior to harvesting and blotting dry. Tissue was lysed in 500 μl of lysis buffer (50 mM Tris-HCl pH 7.2, 10% v/v glycerol, 150 mM NaCl, 1% w/v DIBMA (Anatrace BMA101), with protease inhibitors (1% v/v, Sigma P9599)) and incubated at room temperature for 1 hour with gentle end-over-end mixing. The lysate was centrifuged at 5,000 g for 1 minute and the supernatant filtered through 2 layers of miracloth and combined with an additional 500 μl of filtered lysis buffer (without DIMBA). The clarified lysate was further centrifuged at 16,000 g for 1 minute and the supernatant applied to Amicon 0.5 mL 100 kDa MWCO spin filtration columns and centrifuged at 14,000 g until the retentate was <50 μl. The retentate was diluted to 500 μl with IP buffer (50 mM Tris-HCl pH 7.2, 10% glycerol, 200 mM L-arginine, with protease inhibitor (0.5% v/v, Sigma P9599) and centrifuged at 14,000 g until the retentate was <50 μl. The spin column was inverted and eluted into a 1.5 mL microfuge tube by centrifugation at 100 g for 1 minute The eluate was diluted to 500 μl with IP buffer, of which 20 μl was retained as an input control. Magnetic protein A beads (20 μl per IP reaction) were coated with 5 μg αFLS2 antibody overnight at 4 °C. The resulting beads were washed for 5 minutes with IP buffer containing 0.5 M NaCl followed by 2 washes with IP buffer and resuspended in IP buffer to 100 μl per IP reaction. The resulting FLS2-coated magnetic protein A beads were added to the DIBMA solubilized protein solution and incubated for 3 hours at room temperature with end-over-end mixing. Thereafter, the beads were washed three times with IP buffer, resuspended in 30 μl 2x LDS sample buffer with 2-mercaptoethanol and incubated at 65 °C for 5 minutes with shaking at 1000 RPM. The samples were separated on a 7.5% SDS-PAGE gel prior to transfer to PVDF and western blotting.

Detergent resistant membrane preparation

To evaluate flg22-dependent changes in FLS2 detergent resistant membrane occupancy, 7 seedlings 10 days post-germination were transferred to each well of a 12-well plate, of which each well contained 2 mL 0.5 x MS liquid medium. Seedlings were incubated for 24 hours on an orbital mixer (Luckham R100/TW Rotatest Shaker, 38 mm orbit at 75 RPM), after which 100 μL of 0.5 x MS media containing flg22 was added to give a final flg22 concentration of 10 μM. The seedlings were further incubated with continuous mixing as before for 20 minutes before harvesting and snap freezing in liquid nitrogen. All subsequent steps were performed at 4 °C or on ice. The seedlings were then lysed in 0.5 mL ice cold 1% (v/v) IGEPAL CA-630 in 25 mM Tris-HCl pH 7.4, 150 mM NaCl, 2 mM EDTA, and 0.1% (v/v) protease inhibitors (Sigma-Aldrich, P9599). Lysates were clarified at 500 g and filtered through 1 layer of miracloth. The filtrate was centrifuged at 16,000 g for 30 minutes and the supernatant retained as a detergent soluble fraction (DSM) and mixed 3:1 with 4x reducing (2-mercaptoethanol) LDS sample buffer. The detergent resistant pellet (DRM) was gently washed with 1 mL lysis buffer, centrifuged at 16,000 g for 5 minutes, and the supernatant discarded. The resulting pellet was resuspended in 27 μL of 3:1 lysis buffer: 4x reducing LDS sample buffer, after which 25 μL of the DRM and DSM were separated by 7.5% SDS-PAGE and probed using anti-FLS2 polyclonal antibody as described.[66] Presence of PM H+ ATPase (DRM enriched), Calnexin 1/2 (DSM enriched)[68] and UDP-glucose pyrophosphorylase (cytosol)[69] were used as markers for DRM purity.

Variable Angle - Total Internal Reflection Fluorescence (VA-TIRF) microscopy

VA-TIRF microscopy was performed using an inverted Leica GSD equipped with a 160x objective (NA = 1.43, oil immersion), and an Andor iXon Ultra 897 EMCCD camera. Images were acquired by illuminating samples with a 488 nm solid state diode laser, a cube filter with an excitation filter 488/10 and an emission filter 535/50 for FLS2-GFP, and a 532 nm solid state diode laser, a cube filter with an excitation filter 532/10 and an emission filter 600/100 for mRFP-REM1.3. Optimum critical angle was determined as giving the best signal-to-noise.

Single particle tracking analysis

Nicotiana benthamiana plants (14-21 days old) were infiltrated with *Agrobacterium tumefaciens* (strain GV3101) solution of OD_{600} = 0.5 and imaged 24 to 30 hours post infiltration. Image acquisition was done within 2 to 20 min after 1 μM flg22 or corresponding mock treatment. For single particle tracking experiments, image time series were recorded at 5 frames per second (0.2 s exposure time) by VA-TIRFM. Analyses were carried out as previously described,[70] using the plugin TrackMate7[55] in Fiji.[54] Single particles were segmented frame-by-frame by applying a Laplacian of Gaussian filter and estimated particle size of 0.3 μm. Individual single particle were localized with sub-pixel resolution using a built-in quadratic fitting scheme. Single particle trajectories were reconstructed using a simple linear assignment problem[71] with a maximal linking distance of 0.2 μm and without gap-closing. Only tracks with at least seven successive points (tracked for 1.4 s) were selected for further analysis. Diffusion coefficients of individual particles were extracted using SPTAnalysis[56] based on cosine filtered and maximum likelihood estimates analysis of particles displacement.

Please cite this article in press as: Hurst et al., S-acylation stabilizes ligand-induced receptor kinase complex formation during plant pattern-triggered immune signaling, Current Biology (2023), https://doi.org/10.1016/j.cub.2023.02.065

Co-localization analyses

Nicotiana benthamiana plants (14-21 days old) were infiltrated with *Agrobacterium tumefaciens* (strain GV3101) solution of OD = 0.2 and imaged 48 hours post infiltration. Images were recorded by VA-TIRFM using 250 ms exposure time. As previously reported,[32] we emphasized cluster formation in the presented images by using the 'LoG3D' plugin.[72] Quantitative co-localization analyses of the FLS2-GFP and mRFP-REM1.3 were carried out as previously described,[32] with minor modification. Using FiJi, images were subjected to a background subtraction using the "Rolling ball" method (radius = 20 pixels) and smoothed. We selected regions of TIRF micrographs with homogeneous illumination for both FLS2-GFP and mRFP-REM1.3. The Pearson co-localization coefficients were assessed using the JACoP plugin of FIJI.[73] For comparison, we determined values of correlation, which could be observed by chance by calculating the Pearson coefficient after flipping one of the two images.

Structural modelling of FLS2 kinase domain

The FLS2 intracellular domain (amino acids 831-1173) was submitted to the Phyre2[74] server (http://www.sbg.bio.ic.ac.uk/phyre2/) in default settings. The solved BIR2 kinase domain structure (PDB 4L68, residues 272-600)[75] was identified as the best match and FLS2 residues 841-1171 were successfully modelled onto the BIR2 structure (confidence 100%, coverage 89%). Cys to Ser mutational effects were modelled using Missense3D[76] in default settings.

QUANTIFICATION AND STATISTICAL ANALYSIS

All statistical details relating to specific experiments can be found in relevant Figure legends. In all cases pair-wise comparisons were performed using Student's t-test, comparisons across multiple groups were performed using ANOVA with Tukey's HSD test for significance. Statistical analyses were performed and visualized using R[57] in R-studio.[58]